Mass transfer accompanying coalescence of surfactant-laden and surfactant-free drop in a microfluidic channel

Kovalchuk, Nina M.; Reichow, Marten; Frommweiler, Thomas; Vigolo, Daniele; Simmons, Mark John H.

DOI:
10.1021/acs.langmuir.9b00843

LANGMUIR Article
Cite This: *Langmuir* 2019, 35, 9184–9193
pubs.acs.org/Langmuir

Mass Transfer Accompanying Coalescence of Surfactant-Laden and Surfactant-Free Drop in a Microfluidic Channel

Nina M. Kovalchuk,* Marten Reichow, Thomas Frommweiler, Daniele Vigolo, and Mark J. H. Simmons

University of Birmingham, Edgbaston, Birmingham B15 2TT, U.K.

Supporting Information

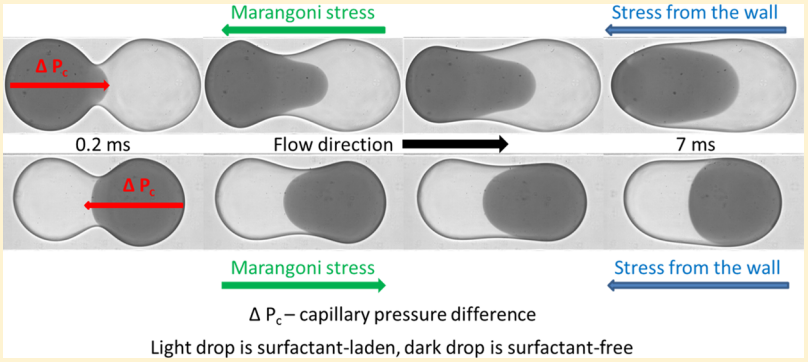

ABSTRACT: The coalescence of two different drops, one surfactant-laden and the other surfactant-free, was studied under the condition of confined flow in a microchannel. The coalescence was accompanied by penetration of the surfactant-free drop into the surfactant-laden drop because of the difference in the capillary pressure and Marangoni flows causing a film of surfactant-laden liquid to spread over the surfactant-free drop. The penetration rate was dependent on the drop order, with considerably better penetration observed for the case when the surfactant-laden drop goes first. The penetration rate was found to increase with an increase of interfacial tension difference between the two drops, an increase of flow rate and drop confinement in the channel (for the case of the surfactant-laden drop going first), an increase of viscosity of the continuous phase, and a decrease of viscosity of the dispersed phase. Analysis of flow patterns inside the coalescing drops has shown that, unlike coalescence of identical drops, only two vortices are formed by asymmetrical coalescence, centered inside the surfactant-free drop. The vortices were accelerated by the flow of the continuous phase if the surfactant-laden drop preceded the surfactant-free one, increasing the rate of penetration; the opposite was observed if the drop order was reversed. The mixing patterns on a longer time scale were also dependent on the drop order, with better mixing being observed for the case when the surfactant-laden drop goes first.

INTRODUCTION

Drop formation, transport, splitting, and coalescence are the main processes used in drop microfluidics.[1−4] The coalescence of drops has received growing attention over the last decade because of many potential applications, with a number of publications providing protocols for tailored drop coalescence using passive[5−7] and active[8−10] methods. Coalescence of identical drops has been studied in microfluidic devices to gain a deeper insight into emulsification processes, either to determine drop stability over a short time scale following drop formation, when adsorption layers of stabilizing agents are not always complete,[11−13] or to estimate the stabilizing properties of surfactants.[14]

The two main advantages provided by coalescence of drops in microfluidics are the possibility to perform chemical reactions under highly controlled conditions and the use of very small amounts of reactants.[2,15] Such microreactors may be separated from each other by the continuous phase, and if reactants and reaction products are soluble only in the dispersed phase, there is no risk of cross-contamination. For example, using 1 mL of sample, it is possible to create thousands to hundreds of thousands of microreactors and thus obtain reliable statistics by varying reaction times and conditions. Other reactants can be added while the drop is moving through the channel, for example, to dilute the sample or quench the reaction. Microfluidic reactors have been successfully used, for example, to measure enzyme kinetic constants[16] or to synthesize nanoparticles[17,18] or hydrogel particles.[19]

A further advantage of microreactors is that their small size leads to small diffusion lengths and thus rapid diffusion of reactants. However, for many applications such as the study of reaction kinetics, the diffusion time is still too large and therefore additional mixing of the drop contents is necessary. If

Received: March 21, 2019
Revised: May 23, 2019
Published: June 21, 2019

DOI: 10.1021/acs.langmuir.9b00843
Langmuir 2019, 35, 9184–9193

one considers the coalescence of two consecutive drops in a straight channel, following coalescence, convective mixing occurs between the front and rear parts of the combined drop. This is driven by the velocity gradient in the direction perpendicular to the channel axis, resulting in two symmetrical convective vortices inside the drop[2,20−22] as the drop moves along the channel. If the drops have different initial compositions, this recirculation mixes the contents of the drops together. According to ref 23, the average striation length decreases to around 15% of the channel size when the drop moves a distance equal to 3 times of its length and shorter drops/plugs mix faster than the longer ones.

Convective mixing can be intensified using chaotic advection, for example, by using serpentine channels.[24] There is however another possibility to intensify mixing by exploiting the properties of coalescing drops: if the interfacial tension of the drops is different, then additional mixing is expected because of the difference of capillary pressure between drops and Marangoni flow. This effect was studied for the coalescence of a drop with a liquid reservoir,[25] drop coalescence in a two-dimensional geometry, where two sessile drops coalesced while spreading over a substrate,[26,27] and in a three-dimensional (3D) geometry, where two spherical drops coalesced in air[28] or in a surrounding viscous liquid.[29−32] For 3D coalescence of two drops, which is the most relevant case for microfluidic applications, it was shown that once the coalescence began, the drop having larger interfacial tension penetrated inside the drop having smaller interfacial tension because of the difference in capillary pressure. At the same time, the difference in the interfacial tension produced Marangoni flow in the direction of higher interfacial tension, so that the drop of lower interfacial tension enveloped the drop with larger interfacial tension. Both phenomena resulted in considerable convective mixing of the drop contents. The penetration velocity and depth were found to increase with the increase of the viscosity of the surrounding liquid[29,30] and the interfacial tension difference.[32]

The study in refs[29,32] was performed in unconfined geometry under conditions of nearly zero flow. If the drops are moving under confinement inside a microfluidic device, mixing due to coalescence will be superimposed upon the recirculatory mixing. Numerical simulations[33] predicted for this case a very sophisticated mixing pattern depending on mutual orientation of flow and interfacial tension gradient. Here, a novel experimental study on coalescence of a surfactant laden and a surfactant-free drop in a microfluidic device is carried out. The mixing patterns after coalescence are studied as a function of the difference in interfacial tension between the drops and the viscosities of the continuous and dispersed phase.

MATERIALS AND METHODS

Decyltrimethylammonium bromide (C_{10}TAB) 99%, Acros Organics; methyl violet dye, Sigma-Aldrich; ultrapure HPLC-grade glycerol, Alfa Aesar; and silicone oils (SO) of viscosity 4.6 and 48 mPa·s, respectively, Aldrich, were used as purchased. Double-distilled water was produced by a water still Aquatron A 4000 D, Stuart.

Drops were generated and coalesced in a microfluidic device made of polydimethylsiloxane (PDMS) using a standard soft lithography procedure.[34] The PDMS geometry was attached to a glass slide with a spin-coated PDMS layer after both were treated by corona discharge for 2 min. The device geometry in the plane of observation is shown in Figure 1. The channels have a rectangular cross section of height h = 170 μm and width w = 360 μm for the input channels and w = 360 and 720 μm, respectively, for the parts of the output channel. The channel width and height were measured directly from microscopic images. To measure height, the PDMS geometry was peeled off the glass slide and cut into slices perpendicular to the plain of observation. The measurements were performed after conditioning the geometry by filling with SO for over 1 week to account for any size changes due to swelling. Coalescence was studied in both the narrow and wide parts of the output channel to account for the effect of confinement.

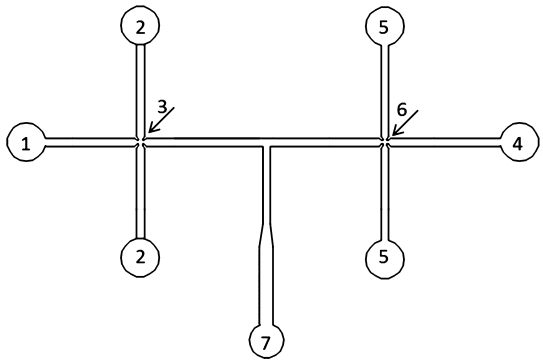

Figure 1. Microfluidic device used in coalescence experiments: 1, 4—input channels for two different dispersed phases, 2, 5—input channels for continuous phase, 3, 6—X-junctions, and 7—output channel.

SO was used as a continuous phase. One of the dispersed phases was water (W) or a surfactant-free mixture of 52 wt % glycerol and water (G_W). The refractive index of the glycerol−water mixture matches that of SO which improves the resolution of velocimetry studies by reducing optical aberrations at the interface between the dispersed and continuous phase. To study the addition of the surfactant, C_{10}TAB was added to the second dispersed phase. To distinguish between the different dispersed phases during the optical measurements and to follow mixing of the drop contents after coalescence, methyl violet dye was added to the surfactant-free dispersed phase at a concentration of 1 g/L. The critical micelle concentration (CMC) in water for C_{10}TAB is 60 mM. Three different surfactant concentrations in water, namely 0.5, 1, and 5 CMC and a single concentration of 5 CMC in G_W, were studied. The properties of continuous and dispersed phases are summarized in Table 1. The addition of methyl violet dye lowers the equilibrium interfacial tension of surfactant-free dispersed phase by 5 mN/m; however, the kinetics of dye adsorption is rather slow, and on the time scale of the microfluidic experiments here described (below 10 s), the decrease is <2 mN/m (estimated from measurements of dynamic surface tension).

Table 1. Properties of the Liquid Pairs Used

continuous phase	viscosity (mPa·s)	dispersed phase	viscosity (mPa·s)	interfacial tension, (mN/m)
SO	4.6	water	1	40
		water + 5 CMC	1	12
SO	48	water	1	36
		water + 0.5 CMC	1	22
		water + 1 CMC	1	14
		water + 5 CMC	1	12
		G_W	6	34
		G_W + 5 CMC	6	12

The liquids were supplied to the microfluidic device by syringe pumps Al-4000 (World Precision Instruments, UK), equipped with 10 mL syringes (BD Plastipak). Drop coalescence was followed using a high-speed video camera (Photron SA-5) connected to an inverted microscope (Nikon Eclipse Ti2-U) at 7000−20 000 fps with an

DOI: 10.1021/acs.langmuir.9b00843
Langmuir 2019, 35, 9184−9193

exposure of 0.02 ms. Both 10× and 20× objectives (Nikon, CFI Plan Fluor DLL) were used giving an image resolution of 2 and 1 μm/pixel, respectively. Image processing was performed using ImageJ free software.[35] All the results obtained are an average of between 3 and 5 experiments.

The flow fields inside the dispersed phase were studied by ghost particle velocimetry (GPV)[22,36−38] using 200 nm polystyrene particles (10% solid, Sigma) added into the dispersed phase at a ratio of 1:50 (v/v). GPV uses as a flow tracer the speckle patterns produced by standard white light scattered by particles smaller than the diffraction limit. The small size of the particles and their low concentration ensured the nonintrusive nature of the measurement. The video recording was carried out at 20 000 fps with an exposure time of 0.05 ms. At least 100 frames were recorded. Images were processed by ImageJ to remove background noise[22] and then analyzed using the open-source MATLAB toolbox PIVlab.[39]

Interfacial tension was measured using a tensiometer K100 (Krüss) equipped with platinum Wilhelmy plate. Parameters for the Langmuir adsorption isotherm were obtained using the software IsoFit[40] available at Ref 41. Dynamic surface tension was measured with a maximum bubble pressure tensiometer (Sinterface).

The viscosity was measured by a TA instruments Discovery-HR-2 rheometer in flow mode using a cone and plate geometry with a cone diameter of 60 mm and an angle of 2° 0′ 29″ with a truncation (gap) of 55 μm.

RESULTS AND DISCUSSION

Characteristic Time Scales. There are several processes that contribute to the mixing accompanying the coalescence of drops with different compositions in a microfluidic device: recirculation inside the coalescing drop because of no-slip conditions on the channel walls, spreading of the content of the surfactant-laden drop over the surface of the surfactant-free drop because of the difference in the interfacial tension between drops, and penetration (intrusion) of the contents of surfactant-free drop into the surfactant-laden drop because of the difference in capillary pressure. The penetration rate in turn depends on the neck kinetics because under the same difference in the capillary pressure between the drops, the liquid velocity inside the neck, that is, the intrusion velocity, depends on the neck cross section. All these processes occur simultaneously and are thus interdependent but have their own characteristic time scales. These depend on system parameters such as flow rates, drop size, channel geometry, liquid viscosities, and surfactant characteristics. Therefore, we first estimate these time scales for the system under consideration without accounting for their probable mutual influence.

The time scale associated with recirculatory flow inside the channel, τ_F, can be calculated as[23]

$$\tau_F = \frac{2L}{U_s} = \frac{LS}{Q_s} \tag{1}$$

where L is the characteristic length scale (the drop radius in the plane of view), U_s is the drop velocity, being close to the flow velocity in the output channel if the drop size is close to that of the channel,[16,38] Q_s in the flow rate in the output channel, and $S = wh$ is the channel cross-sectional area. The experimental flow field inside the plug moving in the microchannel[38] confirms that the recirculation velocity $U_s = O(Q_s/S)$. For the flow rate range used in this study, Q_s = 3−80 μL/min, and the average drop radius, L = 150 μm, thus 5 < τ_F < 200 ms. Note, the characteristic diffusion time, $\tau_D = L^2/D$, where D is the diffusion coefficient. For the considered drop size, τ_D is ∼45 s for a typical value of surfactant diffusion coefficient, $D = 5 \times 10^{-10}$ m^2/s. Therefore, on the time scale of this study (below 100 ms), the contribution of diffusion on mixing can be neglected.

The characteristic time of coalescence depends on the dominant forces. According to ref 42, coalescence initially follows the inertially limited viscous regime with neck radius, r, increasing proportionally to time. This is later replaced by another regime, with slower growth of the neck, proportional to $t^{0.5}$

$$\frac{r}{L} = K\left(\frac{t}{\tau_c}\right)^{0.5} \tag{2}$$

where τ_c is the characteristic time of coalescence and K is a constant close to unity.

Following ref 42, the estimated neck radius at transition from the inertially limited viscous regime in our study should be below 5 μm, that is, below the neck size which can be visualized in this study. Therefore, only the second mentioned regime is expected to be observed. The proportionality coefficient to $t^{0.5}$, defining the characteristic time scale of coalescence, depends on the properties of the continuous and dispersed phases. The analysis of the results for drops of radius 1−2 mm in unconfined geometry carried out in ref 42 has shown that if $\mu_c/\sqrt{\rho\sigma L} > 0.3$, then coalescence follows the regime mediated by the viscosity of the continuous phase with a characteristic time scale

$$\tau_{cv} = \frac{\mu_c L}{\sigma} \tag{3a}$$

where μ_c is the dynamic viscosity of the continuous phase, σ is the interfacial tension, and ρ is the density of the denser liquid, which is the dispersed phase in the case considered here.

If $\mu_c/\sqrt{\rho\sigma L} < 0.3$, then coalescence proceeds in the inertial regime governed by dispersed phase (being more dense) with a characteristic time scale[42]

$$\tau_{ci} = L\sqrt{\frac{L\rho}{\sigma}} \tag{3b}$$

For drop radius L = 150 μm, the viscous regime is expected for μ_c > 23 mPa·s for the surfactant-free system (σ = 40 mN/m) and for μ_c > 13 mPa·s for the smallest interfacial tension used (σ = 12 mN/m). Therefore, for all compositions of dispersed phase, the viscous regime of coalescence is expected for viscosity of the continuous phase equal to 48 mPa·s, whereas the inertial regime is expected for viscosity of the continuous phase of 4.6 mPa·s. Estimation of corresponding time scales by eqs 3a and 3b gives 0.2 < τ_{cv} < 0.6 ms and 0.3 < τ_{ci} < 0.5 ms, that is, surprisingly both viscous and inertial time scales are similar for the liquids used in this study.

The characteristic time for mixing driven by capillary pressure difference between the drops having different interfacial tension is

$$\tau_P = \frac{8\mu_d L}{\Delta\sigma} \tag{4}$$

which gives for conditions used in this study 0.04 < τ_p < 0.10 ms if water is used as the dispersed phase and $\tau_p \approx 0.36$ ms for the glycerol−water mixture. Comparing the time scales of capillary pressure driven flow, eq 4, coalescence, eq 3a, and recirculation, eq 1, one can expect mass transfer inside the coalesced drop because of the pressure difference on the time scale of coalescence; this mass transfer can be affected by

DOI: 10.1021/acs.langmuir.9b00843
Langmuir 2019, 35, 9184−9193

recirculation at high flow rates, whereas at small flow rates, mixing should be driven mainly by the capillary pressure flow.

Capillary pressure driven flow will persist as long as there is a difference in the interfacial tension between drops. This difference gives rise to Marangoni flow once the drops contact each other. The Marangoni flow, on the one hand, contributes to mixing between the coalescing drops but, on the other hand, transfers the surfactant over the surface of the initial surfactant-free drop, which results in a more uniform surfactant distribution and diminishing of capillary pressure difference. As the Marangoni flow involves adjacent to the interface layers in both continuous and dispersed phases, its time scale depends on the viscosities of both phases and can be defined as

$$\tau_M = \frac{(\mu_c + \mu_d)L}{\Delta\sigma} \tag{5}$$

where μ_d is the dynamic viscosity of dispersed phase and $\Delta\sigma$ is the difference in the interfacial tension between drops. One can calculate that for μ_c = 48 mPa·s, μ_d = 6 mPa·s and $\Delta\sigma$ = 22 mN/m (G_W in more viscous SO), $\tau_M \approx 0.4$ ms, and for μ_c = 4.6 mPa·s, μ_d = 1 mPa·s, and $\Delta\sigma$ = 28 mN/m (water in less viscous SO), $\tau_M \approx 0.03$ ms, that is, it is similar to the time scale of drop coalescence. This means that the Marangoni flow will contribute to mixing on the time scale of coalescence, but it can reduce considerably the contribution from the capillary pressure driven mixing because of the reduction of the difference in interfacial tension between the drops. The extent of interfacial tension equilibration due to Marangoni flow depends, however, on the surfactant properties. As the surfactant is soluble in the dispersed phase, it will adsorb on the side of the initially surfactant-laden drop and desorb on the side of the initially surfactant-free drop.

The characteristic time scale for interfacial tension relaxation can be calculated as[43,44]

$$\tau_\sigma = \frac{2(d\Gamma/dc)^2}{D} \tag{6}$$

where Γ is the surface adsorption and c is the surfactant concentration. Assuming that the adsorption kinetics is diffusion controlled and using Langmuir adsorption isotherm

$$\Gamma = \Gamma_\infty \frac{bc}{1 + bc} \tag{7}$$

Equation 6 can be rewritten as

$$\tau_\sigma = \frac{2}{D}\left(\frac{\Gamma_\infty b}{(1 + bc)^2}\right)^2 \tag{6a}$$

where Γ_∞ is the limiting adsorption and b is the Langmuir adsorption constant. Γ_∞ and b was found from fitting the experimentally measured dependence of interfacial tension on concentration for the fluid pair of water and 48 mPa·s SO (Figure S1) according to the Szyszkowski–Langmuir equation

$$\sigma = \sigma_0 + RT\Gamma_\infty \ln(1 + bc) \tag{8}$$

as $b = 2.6 \times 10^{-2}$ m^3/mol and $\Gamma_\infty = 9.1 \times 10^{-6}$ mol/m^2.

According to the literature,[45−47] the aggregation number for C_{10}TAB is in the range 30–40; therefore, for calculations, we have chosen N_a = 35. Then, for the 5 CMC solution of C_{10}TAB, $D_{eff} \approx 5 \times 10^{-9}$ m^2/s and $\tau_\sigma < 0.1$ μs. In this case, surfactant replenishment at the interface from the surfactant-laden side and surfactant desorption on the surfactant-free side should be practically instantaneous and the surface tension gradient will be supported as long as there remains a considerable difference in the bulk concentration of the surfactant between the drops. Equilibration of the bulk concentration in this study occurs on the time scale of tens of milliseconds, see section Mixing on Long Time Scale and in particular Figure 10.

Note that such a fast relaxation is a specific characteristic of C_{10}TAB because of its high CMC value and small activity (constant b in eq 8). This surfactant was deliberately chosen to keep the surface tension gradient unchanged during the coalescence process. For other low-molecular-weight surfactants, especially nonionic, this relaxation time can be of the order of tens of milliseconds at the CMC and in the seconds range and higher at concentrations below the CMC.[44]

Neck Kinetics. Because surface tension at the neck is a crucial parameter in defining the neck kinetics, the surfactant-free dispersed phase was used to account for the effect of flow conditions and viscosity of the continuous phase on the coalescence kinetics in a microchannel in order to avoid any influence of surfactant redistribution. Figure 2 shows the time evolution of the neck radius by coalescence of water drops in 48 mPa·s viscosity SO. The neck radius was normalized by the drop radius and time was normalized by the characteristic viscous time τ_{cv} to account for the variation in drop sizes (in the range 271–298 μm). Note that the velocity in the wide channel at Q_s = 98 μL/min is similar to the velocity in the narrow channel at Q_s = 43 μL/min because of the twice larger cross-sectional area of the wide channel.

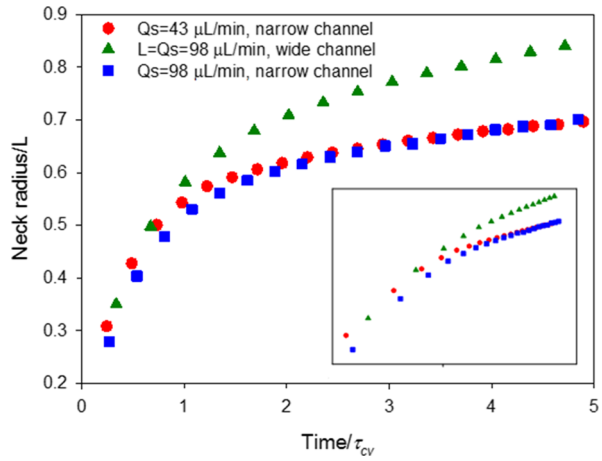

Figure 2. Kinetics of neck growth at coalescence of two surfactant-free drops of water in SO 48 mPa·s under different flow conditions. Axis labels in the inset are the same as in the main graph.

According to Figure 2, the superficial flow rate in the channel does not have a considerable effect on the neck kinetics, but the rate of confinement does. All three curves show similar early kinetics on a time scale up to 1 and for the dimensionless neck radius up to 0.5 with the power law exponent being in the range 0.44–48 for all three cases, consistent with predicted scaling for the neck radius in eq 2. The coefficient K in eq 2 was found to be 0.55 ± 0.02 for coalescence in the narrow channel and 0.60 ± 0.02 for coalescence in the wide channel. It can be assumed that this difference in K values is due to larger confinement in the narrow channel, making the redistribution of continuous phase more difficult.

DOI: 10.1021/acs.langmuir.9b00843
Langmuir 2019, 35, 9184–9193

At $R/L > 0.5$, the kinetics slow down in agreement with previous observations reported for unconfined geometry.[32,42] In the confined geometry considered here, the slowing down is more pronounced than in refs[32,42] and depends on the degree of confinement. For coalescence in the narrow channel, where the ratio of drop diameter to channel width was around 0.8, the power law exponent for the slow neck kinetics was ~0.15, whereas for wide channel with two times smaller confinement, it was ~0.21. This behavior is in line with the dependence of K on confinement.

The comparison of coalescence of surfactant-free drops at respective continuous phase viscosities of 4.6 and 48 mPa·s shown in Figure S2 illustrates that the neck grows much faster in the less viscous oil despite the similarity of viscous and inertial time scales discussed above. This is the result of the difference in the coefficient K, which for inertial kinetics at μ_c = 4.6 mPa·s is ~0.9, that is, in the case of low-viscosity oil and inertial kinetics, the effect of confinement is rather small.

When the coalescing drops have different interfacial tensions because of the presence of a surfactant, their contact results in large gradients of interfacial tension and transfer of surfactant from the surfactant-laden drop to the surfactant-free drop by the interfacial (Marangoni) flow. The surfactant and velocity distribution over the interface is governed by the coupled hydrodynamics and the mass transfer is strongly nonlinear and changes with time.[48] The coalescence kinetics, at least on the short time scale when it follows eq 2, is determined mostly by the surfactant concentration at the neck. The last is hardly predictable a priori from the simple time-scale analysis because many forces are involved locally.

Figure 3 compares the neck kinetics for the coalescence of one surfactant-laden drop and one surfactant-free drop with

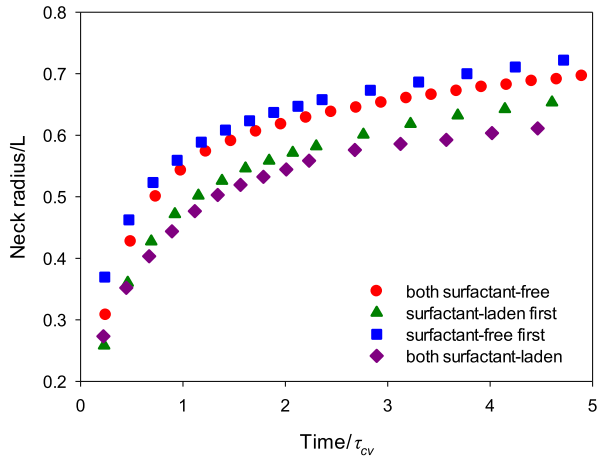

Figure 3. Kinetics of neck growth during coalescence of two aqueous drops of different compositions (see legend), in the narrow channel. The surfactant-laden drop contains 5 CMC of C_{10}TAB; continuous phase—SO 48 mPa·s; flow rate in the output channel—27 μL/min; τ_{cv} for all the curves is based on the interfacial tension of the surfactant-free system, σ = 36 mN/m.

the kinetics of two surfactant-laden drops and two surfactant-free drops. For the case of coalescence of two different drops, two cases are considered: the surfactant-laden drop being either at the front or behind as the drops flow down the channel. In the former case, the difference in capillary pressure, Marangoni stress, and shear stress from the motionless channel wall acts in the same direction, whereas for the latter, the shear stress from the wall opposes the two other forces.

There is a distinctive difference in the neck kinetics between the coalescence of two surfactant-laden drops and two surfactant free drops, the former being slower, as expected. In the case when the surfactant-laden drop is at the front, the kinetics is close to that of two surfactant-laden drops. Therefore, it can be assumed that the surfactant concentration at the neck is close to the CMC value in this case. In the case when the surfactant-laden drop goes last (behind), the kinetics is close to that of two surfactant-free drops and it can be assumed that there is practically no surfactant at the neck in this case. The difference in kinetics due to the drop order was also observed for concentrations of C_{10}TAB of 0.5 CMC and 1 CMC. Thus, it can be concluded that despite the much larger global time scale of the recirculatory flow resulting from the drop interaction with the channel wall as compared with the Marangoni time scale, the wall shear stress affects considerably the surfactant redistribution after coalescence of the surfactant-laden and surfactant-free drop. It will be shown below that it also affects the mixing patterns inside the coalescing drops.

Mass Transfer on Short Time Scale. At coalescence incipience, there is a considerable difference in the capillary pressure between the surfactant-laden drop and the surfactant-free drop because of the difference in interfacial tension. As stated above, this results in the penetration of the surfactant-free drop into the surfactant-laden one as shown in Figure 4

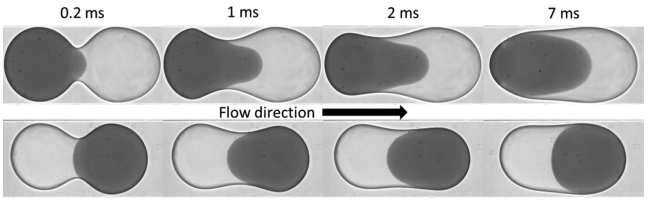

Figure 4. Mass transfer between drops accompanying their coalescence. The surfactant-free drop is an aqueous solution of methyl-violet dye, the surfactant-laden drop is an aqueous solution of 300 mM (5 CMC) C_{10}TAB, the continuous phase is SO 48 mPa·s; flow rate in the output channel—27 μL/min (corresponds to the conditions shown in Figure 3). Top row—surfactant-laden drop goes first, the diameter of surfactant-laden drop D_{SL} = 340 μm, the diameter of surfactant-free drop D_{SF} = 327 μm; bottom row—surfactant-free drop goes first, D_{SF} = 310 μm, D_{SL} = 291 μm.

(Videos S1 and S2) for two drops coalescing in 48 mPa·s SO. The penetration kinetics is quantified in Figure 5, where each curve represents the averaged data from three to four drops. In Figure 5, the maximum penetration length of surfactant-free phase is normalized by the full length of coalesced drop as shown in the top left inset. Such normalization accounts for changes in the length because of the change of the coalesced drop shape.

The characteristic time of recirculatory mixing for coalescence presented in Figures 4 and 5 is $\tau_F \approx 20$ ms. However, it is clearly visible that there is a considerable dependence of the intrusion length on the drop order. On the short time scale of $t \approx 1$ ms, penetration is considerably stronger when surfactant-laden drop goes first. Note that for this case, there is a noticeable dependence of the penetration kinetics on the interfacial tension: increase of surfactant concentration from 0.5 CMC to 1 CMC (i.e., increase in interfacial tension difference between drops from 12 to 22

DOI: 10.1021/acs.langmuir.9b00843
Langmuir 2019, 35, 9184−9193

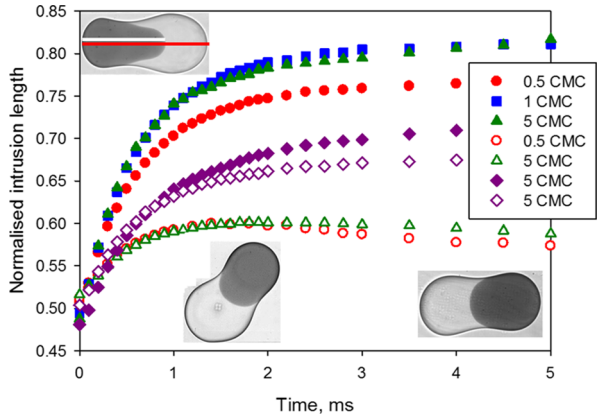

Figure 5. Dependence of intrusion length of the content of the surfactant-free water drop into the surfactant-laden water drops on time. The continuous phase is SO 48 mPa·s. Filled symbols correspond to the surfactant-laden drop followed by the surfactant-free one (top inset); empty symbols correspond to the surfactant-laden drop, followed by the surfactant-free one (bottom right inset). Diamonds represent coalescence in the wide channel at Q_s = 20 μL/min (bottom left inset), all other symbols represent coalescence in the narrow channel at Q_s = 44–48 μL/min. The intrusion length is normalized by the total length of the coalescing drop as shown in the top inset.

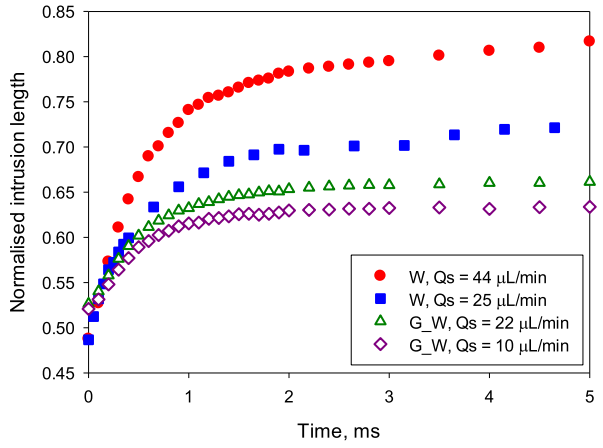

Figure 6. Dependence of penetration length (surfactant-laden drop of 5 CMC C_{10}TAB goes first) on flow velocity in the output channel. Filled symbols correspond to water as the dispersed phase and empty symbols correspond to the glycerol–water mixture as the dispersed phase. The continuous phase is SO 48 mPa·s.

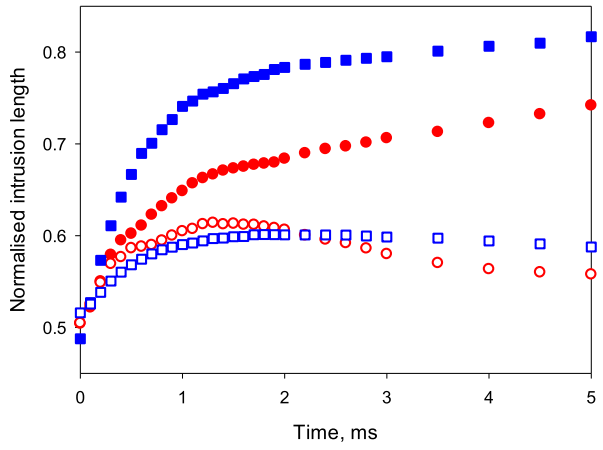

Figure 7. Effect of viscosity of the continuous phase on the intrusion length: circles—continuous phase 4.6 mPa·s, Q_s = 42 μL/min; squares—continuous phase 48 mPa·s, Q_s = 44 μL/min. The dispersed phase is water. Filled symbols correspond to the surfactant-laden (5 CMC) drop followed by the surfactant-free one, empty symbols correspond to the opposite drop order.

mN/m) results in faster penetration rate and larger penetration depth. Interfacial tension decreases only by 2 mN/m with an increase of concentration from 1 CMC to 5 CMC; therefore, the penetration kinetics for these two concentrations are practically the same.

When the drops enter the wide channel, they align pairwise at an angle ~45° to the channel axis as shown in the bottom left inset shown in Figure 5. In this case, the penetration kinetics slow down in comparison to the narrow channel for the case when the surfactant-laden drop goes first and accelerates as compared to the narrow channel for the reversed drop order. The dependence of the penetration on the drop order in the wide channel is close to the experimental error. Note that unlike the neck kinetics, the penetration kinetics depends on the superficial flow rate, as shown in Figure 6. Therefore, to a large extent, the difference in penetration between the narrow and wide channels is due to difference in the flow conditions.

According to eq 4, the penetration kinetics should depend strongly on the viscosity of the dispersed phase. Indeed, this is confirmed by the comparison of the penetration kinetics by the coalescence of surfactant-laden and surfactant-free drops of water and those of glycerol–water as shown in Figure 6. Penetration kinetics also depends on the viscosity of continuous phase as shown in Figure 7. This dependence is mostly due to the difference in the neck kinetics. For the less viscous continuous phase, the neck diameter increases faster (Figure S2); therefore, the penetrating surfactant-free phase has to fill the larger cross-sectional area, which results in a smaller penetration length.

An increase of the neck radius provides a negative contribution to the length of both the coalesced drop and its surfactant-free part. As shown in Figure S3, this contribution results in the continuous decrease of the full drop length, whereas the length of the surfactant-free part of the drop first increases due to penetration. Later, a negative contribution from the shape change exceeds the contribution from the penetration and the length of the surfactant-free part begins to decrease. For the case presented in Figure 4, the fastest penetration occurs within 0.5 ms with an average intrusion velocity of 150 mm/s if the surfactant-laden drop goes first and 63 mm/s for the opposite drops order. The full length of the drop decreases faster in the case when a surfactant-laden drop goes first. This is the result of increasing asymmetry in the drop shape (top row in Figure 4): the content of the surfactant-free part is squeezed out, decreasing the radius of the surfactant-free part and increasing the radius of the surfactant-laden part. This asymmetry also affects the penetration length, first, by making the surfactant-free part more elongated and, second, by an increase of the capillary pressure difference.

Figure 8 presents the flow fields inside the surfactant-laden and surfactant-free coalescing drops containing glycerol–water, which is used to match the refractive index with the SO and enable improved flow resolution near the drop interfaces. Video S3 shows the movement of the speckle pattern visualizing the flow inside the coalescing drops. The

DOI: 10.1021/acs.langmuir.9b00843
Langmuir 2019, 35, 9184–9193

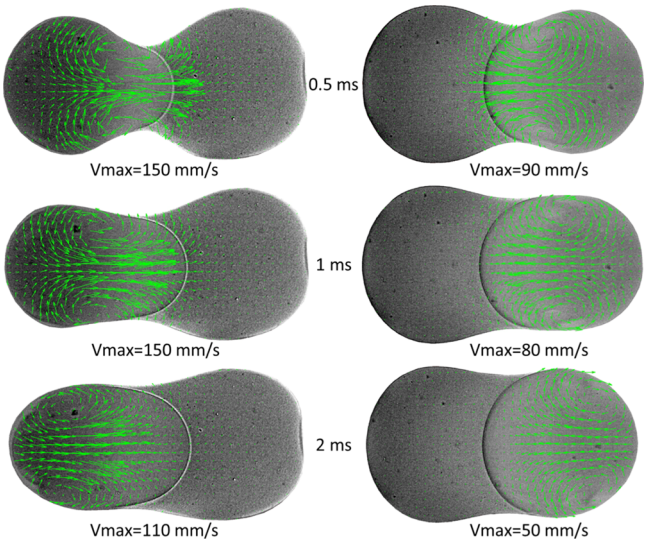

Figure 8. Flow fields inside the coalescing drops. Surfactant-free drop—mixture of 52% glycerol and 48% water (v/v), surfactant-laden drop—300 mM solution of C_{10}TAB in glycerol–water mixture, continuous phase—SO 48 mPa·s; flow rate in the output channel—22 μL/min. The average velocity inside the drops before coalescence (8 mm/s) was subtracted from the flow. First column—surfactant-laden drop goes first, the diameter of surfactant-laden drop D_{SL} = 299 μm, the diameter of surfactant-free drop D_{SF} = 277 μm; second column—surfactant-free drop goes first, D_{SF} = 290 μm, D_{SL} = 300 μm.

penetration kinetics for a similar pair of drops is shown in Figure 6.

The coalescence gives rise to two different types of flow: the Marangoni flow due to the gradient of the interfacial tension between the drops and the bulk flow due to the difference in the capillary pressure between the drops and the neck and between the drops themselves. The Marangoni flow is generated at the interface, and it also causes movement of the bulk fluid directed from the surfactant-laden drop to the surfactant-free drop. The capillary pressure driven flow is directed from the surfactant-free drop into the surfactant-laden drop with a maximum velocity along the axis connecting the centers of the drops. This is shown in Figure 8 and from the velocity distribution along the penetration line presented in Figure S4. It should be stressed that the main driving force of this flow is the difference in capillary pressure between the drops and the neck region. The flow results in the increase of neck diameter and is observed in any coalescence event including coalescence of similar drops;[42,49] however, the flow structure is strikingly different between the coalescence of similar and dissimilar drops.

In the case of coalescence of similar drops, both drops contribute equally to the liquid inflow into the neck. Therefore, the increase in the neck diameter is accompanied by the formation of four symmetrical convective vortices in relation to the middle plane between the drops and the center to center axis in a Lagrangian coordinate system moving along the channel axis with the drops at the flow velocity.[38] As expected for the symmetrical case, the velocity vectors do not cross the middle plane between the drops; that is, there is no mass transfer between the drops.

In the case when drops have different interfacial tension, there is a capillary pressure difference not only between the drops and the neck but also between the two drops. Therefore, the neck filling in this case occurs by the liquid from the drop having larger capillary pressure (i.e., larger interfacial tension). The liquid from this drop not only fills the neck but also penetrates into the bulk of the second drop. This results in the formation of only two convective vortices because of the motion of the liquid from the drop with higher interfacial tension, whereas the liquid from the distant part of the drop with lower interfacial tension moves with a velocity close to the flow velocity.

The maximum velocity to be reliably derived from GPV can be estimated as $U = L_{IR}/4\Delta t$, where L_{IR} is the length of interrogation region and Δt is the time between the successive frames in video-recording.[37] The minimum Δt in this study was 0.05 ms and L_{IR} = 32 μm, which gives the maximum velocity U = 160 mm/s. Therefore, because of the limitation of the high-speed camera used in this study, it was not possible to obtain flow patterns at t < 0.5 ms; even at t = 0.5 ms, there is a large error in the flow vectors for the case when the surfactant-laden drop goes first.

It was observed, for symmetrical drop coalescence,[38] that the movement of coalesced drop along the channel results in the vortex symmetry breaking because of their interaction with the continuous phase: the vortex in the first moving drop is retarded, whereas vortex in the second moving drop is enhanced. The same is observed in the case of asymmetrical drop coalescence with the only difference being that the vortices are always located in the surfactant-free drop. Thus, if the surfactant-free drop goes second (see the first column in Figure 8), the vortices are enhanced by the interaction with the flow in the channel, whereas for the surfactant-free drop going first (see the second column in Figure 8), the vortices are retarded. This explains the dependence of the maximum velocity inside the drop and therefore the penetration rate on the order of the drops.

With time, the centers of the vortices move to the rear part of the coalesced drop, which results in a decrease of the penetration velocity as can be seen from Figure S4. Such a vortex movement was also observed for the case of symmetrical coalescence,[38] but in the asymmetrical case, it occurs much faster. It can be assumed that acceleration in the movement of the vortices centers is due to the propagation of the Marangoni flow. The time scale of Marangoni flow for the system presented in Figures 8 and S4 is $\tau_M \approx 0.4$ ms, that is, comparable with the time scale of observation. The propagation of Marangoni flow can be seen in Video S3.

Mixing on Long Time Scale. As shown in the previous subsection, the mixing of the drop content due to asymmetry in capillary pressure occurs on a millisecond time scale. At a time scale of tens of milliseconds, the mixing continues by recirculation inside the coalesced drop because of a gradient of longitudinal velocity over the channel cross section (see subsection Characteristic Time Scales). The initial conditions for this recirculatory mixing are defined by the penetration pattern built on the smaller time scale.

Figure 9 and Video S4 present the mixing patterns inside the coalescing drop on a time scale ranging from 10 to 50 ms at the maximum studied flow rate of 80 μL/min. At this flow rate, the characteristic time of recirculatory mixing (eq 1) is τ_F = 5 ms; therefore, well-developed mixing patterns can be seen in Figure 9. It is obvious from Figure 9 that much better mixing is achieved for the case when surfactant-laden drop goes first.

There are several approaches for the quantification of mixing using image analysis.[9,50] Here, a simplified version of mixing index[50] was used. The mixing efficiency was calculated as the

DOI: 10.1021/acs.langmuir.9b00843
Langmuir 2019, 35, 9184–9193

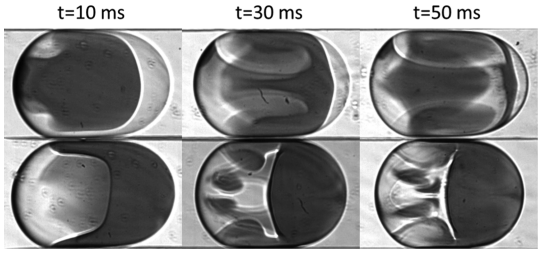

Figure 9. Mixing patterns following the coalescence of dyed surfactant-free drop of water and surfactant-laden (C10TAB, 5 CMC) drop: viscosity of continuous phase μ_c = 4.8 mPa·s, flow velocity in the output channel Q_s = 80 μL/min. Top row—surfactant-laden drop goes first, bottom row—surfactant-free drop goes first. The height of each picture is equal to the channel width, 360 μm.

difference in average gray values between the front and the rear halves of coalesced drop normalized by the gray scale value in the same part of channel filled by continuous phase (Figure 10). This simple method gives a reasonable estimation of the mixing efficiency.

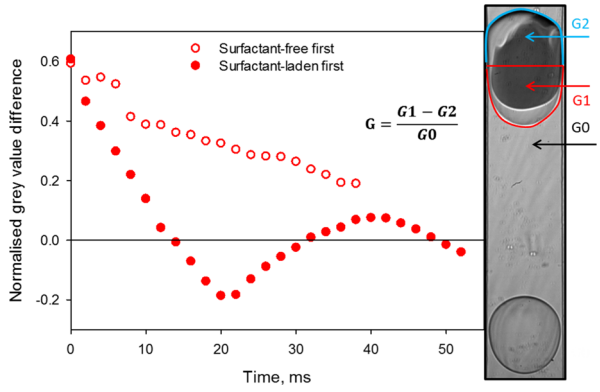

Figure 10. Mixing kinetics presented by normalized gray value difference following the coalescence of a dyed surfactant-free drop of water and a surfactant-laden (C10TAB, 5 CMC) drop of water. Viscosity of continuous phase μ_c = 4.8 mPa·s, flow velocity in the output channel Q_s = 80 μL/min.

Figure 10 confirms the visual observation from Figure 9 that the mixing occurs much faster for the case when surfactant-laden drop goes first. Obviously, the chosen estimation method gives only the average difference between two parts of the drop and zero value of the intensity difference does not mean perfect mixing. Figure 10 shows that after reaching the first zero, the intensity difference oscillates around it. The further mixing results in the decrease of the oscillation amplitude before the complete mixing is achieved.

CONCLUSIONS

Mass transfer following the asymmetric coalescence of two drops was studied in a microfluidic device. The asymmetry was the result of the presence of surfactant only in one of the coalescing drops. The coalescence of surfactant-laden drop and surfactant-free drop is accompanied by the penetration of the content of the drop with higher interfacial tension into the drop of lower interfacial tension. The rate of penetration crucially depends on the drop order: it is much larger when the surfactant-laden drop goes first. The penetration rate increases with an increase of interfacial tension difference, increase of flow rate and drop confinement in the channel (for the case of a surfactant-laden drop followed by a surfactant-free one), increase of viscosity of the continuous phase, and decrease of viscosity of the dispersed phase.

The contact of two drops results in a Marangoni flow directed on the interface from the surfactant-laden drop toward the surfactant-free drop. This flow redistributes the surfactant and therefore can change the neck kinetics by changing the interfacial tension at the neck. Under the conditions of this study, the neck kinetics for the case when the surfactant-free drop was followed by the surfactant-laden one was close to the neck kinetics observed for coalescence of two surfactant-free drops and was close to the kinetics of two surfactant-laden drops for the opposite drop order.

The flow patterns inside the coalescing drop for asymmetric coalescence (drops of the different interfacial tension) differ considerably from the symmetric case (drops of the same interfacial tension). In the symmetric case, coalescence resulted in the formation of four symmetrical vortices,[38] whereas in the asymmetrical case, only two vortices were formed with the centers inside the surfactant-free drop. Those vortices contributed to both the neck growth and the penetration of the content of surfactant-free drop into the surfactant-laden one. The vortices in the first drop along the flow direction are retarded by the flow of the continuous phase, whereas the vortices in the second drop are enhanced. This is the reason why a higher penetration rate has been observed for the case when the surfactant-laden drop goes first.

Theoretical analysis has shown that there are two time scales for mixing of coalescing drops under flow conditions in a microchannel. Processes such as coalescence, Marangoni flow, and mixing due to difference in capillary pressure between drops acted on the fast time scale of the order of 0.1−1 ms. The characteristic time scale for the mixing caused by the recirculatory flow due to the velocity gradients over the channel cross-section was of the order of tens of milliseconds. The mixing patterns on the time scale of tens of milliseconds also depend on the drop order. Faster mixing is achieved if the surfactant-laden drop goes first.

ASSOCIATED CONTENT

Supporting Information

The Supporting Information is available free of charge on the ACS Publications website at DOI: 10.1021/acs.langmuir.9b00843.

Isotherm of interfacial tension of C_{10}TAB at water/SO 48 mPa·s interface; kinetics of neck growth at coalescence of two surfactant-free drops of water in SOs of different viscosities at flow rate 98 mL/min in a narrow channel; comparison of kinetics of the maximum length of the coalesced drop (empty symbols) and its surfactant-free part (filled symbols) for coalescence of a surfactant-free drop with a drop of solution C_{10}TAB (5 CMC) in SO 48 mPa·s; circles—surfactant-laden drop goes first, squares—surfactant-free drop goes first; length is normalized by the initial drop size; distribution of the longitudinal velocity component in the liquid bulk along the interface between the surfactant-free phase and the surfactant-laden phase (seen as a line inside the coalesced drop shown in Figure 8); positive value of velocity corresponds to the direction of penetration; circles correspond to the case when surfactant-laden

DOI: 10.1021/acs.langmuir.9b00843
Langmuir 2019, 35, 9184−9193

drop goes first, squares—surfactant-free drop goes first (PDF)

Coalescence of a surfactant-free aqueous drop dyed with methyl violet (dark) with a surfactant-laden drop (light) of an aqueous solution of 300 mM C_{10}TAB; continuous phase is SO 48 mPa·s; flow rate in the output channel—27 μL/min; surfactant-laden drop goes first; video corresponds to the set of images in the top row of Figure 4 (MP4)

Coalescence of a surfactant-free aqueous drop dyed with methyl violet (dark) with a surfactant-laden drop (light) of an aqueous solution of 300 mM C_{10}TAB; the continuous phase is SO 48 mPa·s; flow rate in the output channel—27 μL/min; surfactant-laden drop goes second; video corresponds to the set of images in the bottom row of Figure 4 (MP4)

Speckle patterns visualizing the flow fields inside the coalescing drops; surfactant-free drop—mixture of 52% glycerol and 48% water (v/v), surfactant-laden drop—300 mM solution of C_{10}TAB in glycerol–water mixture, continuous phase—SO 48 mPa·s; flow rate in the output channel—22 μL/min; video corresponds to the first column in Figure 8 (surfactant-laden drop goes first) (MP4)

Mixing following the coalescence of dyed surfactant-free drop of water and surfactant-laden (C_{10}TAB, 5 CMC) drop: viscosity of continuous phase μ_c = 4.8 mPa·s, flow velocity in the output channel Q_s = 80 μL/min; surfactant-laden drop goes first; video corresponds to the top row in Figure 9 (MP4)

AUTHOR INFORMATION

Corresponding Author

*E-mail: n.kovalchuk@bham.ac.uk.

ORCID

Nina M. Kovalchuk: 0000-0002-6497-650X

Notes

The authors declare no competing financial interest.

ACKNOWLEDGMENTS

This work is funded by the EPSRC Programme Grant "MEMPHIS—Multiscale Examination of Multiphase Physics in Flows" (EP/K003976/1) and the Royal Society Research Grant 2017 R1 (RG160698). M.R. and T.F. acknowledge the University of Birmingham for financial support of their summer research projects.

REFERENCES

(1) Baroud, C. N.; Gallaire, F.; Dangla, R. Dynamics of microfluidic droplets. *Lab Chip* **2010**, *10*, 2032–2045.

(2) Seemann, R.; Brinkmann, M.; Pfohl, T.; Herminghaus, S. Droplet based microfluidics. *Rep. Prog. Phys.* **2012**, *75*, 016601.

(3) Pit, A.; Duits, M.; Mugele, F. Droplet Manipulations in Two Phase Flow Microfluidics. *Micromachines* **2015**, *6*, 1768–1793.

(4) Dressler, O. J.; Casadevall i Solvas, X.; deMello, A. J. Chemical and Biological Dynamics Using Droplet-Based Microfluidics. *Annu. Rev. Anal. Chem.* **2017**, *10*, 1–24.

(5) Niu, X.; Gulati, S.; Edel, J. B.; deMello, A. J. Pillar-induced droplet merging in microfluidic circuits. *Lab Chip* **2008**, *8*, 1837–1841.

(6) Lee, S.; Kim, H.; Won, D.-J.; Lee, J.; Kim, J. On-demand, parallel droplet merging method with non-contact droplet pairing in droplet-based microfluidics. *Microfluid. Nanofluid.* **2016**, *20*, 1–15.

(7) Fidalgo, L. M.; Abell, C.; Huck, W. T. S. Surface-induced droplet fusion in microfluidic devices. *Lab Chip* **2007**, *7*, 984–986.

(8) Dunkel, P.; Hayat, Z.; Barosi, A.; Bchellaoui, N.; Dhimane, H.; Dalko, P. I.; et al. Photolysis-driven merging of microdroplets in microfluidic chambers. *Lab Chip* **2016**, *16*, 1484–1491.

(9) Sarrazin, F.; Prat, L.; Di Miceli, N.; Cristobal, G.; Link, D. R.; Weitz, D. A. Mixing characterization inside microdroplets engineered on a microcoalescer. *Chem. Eng. Sci.* **2007**, *62*, 1042–1048.

(10) Sun, J.; Wang, W.; He, F.; Chen, Z.-H.; Xie, R.; Ju, X.-J.; et al. On-chip thermo-triggered coalescence of controllable Pickering emulsion droplet pairs. *RSC Adv.* **2016**, *6*, 64182–64192.

(11) Baret, J.-C.; Kleinschmidt, F.; El Harrak, A.; Griffiths, A. D. Kinetic aspects of emulsion stabilization by surfactants: a microfluidic analysis. *Langmuir* **2009**, *25*, 6088–6093.

(12) Muijlwijk, K.; Colijn, I.; Harsono, H.; Krebs, T.; Berton-Carabin, C.; Schroën, K. Coalescence of protein-stabilised emulsions studied with microfluidics. *Food Hydrocolloids* **2017**, *70*, 96–104.

(13) Riechers, B.; Maes, F.; Akoury, E.; Semin, B.; Gruner, P.; Baret, J.-C. Surfactant adsorption kinetics in microfluidics. *Proc. Natl. Acad. Sci. U.S.A.* **2016**, *113*, 11465–11470.

(14) Krebs, T.; Schroën, K.; Boom, R. Coalescence dynamics of surfactant-stabilized emulsions studied with microfluidics. *Soft Matter* **2012**, *8*, 10650.

(15) Kaminski, T. S.; Garstecki, P. Controlled droplet microfluidic systems for multistep chemical and biological assays. *Chem. Soc. Rev.* **2017**, *46*, 6210–6226.

(16) Ahn, K.; Agresti, J.; Chong, H.; Marquez, M.; Weitz, D. A. Electrocoalescence of drops synchronized by size-dependent flow in microfluidic channels. *Appl. Phys. Lett.* **2006**, *88*, 264105.

(17) Frenz, L.; El Harrak, A.; Pauly, M.; Bégin-Colin, S.; Griffiths, A. D.; Baret, J.-C. Droplet-based microreactors for the synthesis of magnetic iron oxide nanoparticles. *Angew. Chem., Int. Ed. Engl.* **2008**, *47*, 6817–6820.

(18) Hung, L.-H.; Choi, K. M.; Tseng, W.-Y.; Tan, Y.-C.; Shea, K. J.; Lee, A. P. Alternating droplet generation and controlled dynamic droplet fusion in microfluidic device for CdS nanoparticle synthesis. *Lab Chip* **2006**, *6*, 174–178.

(19) Liu, K.; Ding, H.; Chen, Y.; Zhao, X.-Z. Droplet-based synthetic method using microflow focusing and droplet fusion. *Microfluid. Nanofluid.* **2007**, *3*, 239–243.

(20) Sarrazin, F.; Loubière, K.; Prat, L.; Gourdon, C.; Bonometti, T.; Magnaudet, J. Experimental and numerical study of droplets hydrodynamics in microchannels. *AIChE J.* **2006**, *52*, 4061–4070.

(21) Rhee, M.; Burns, M. A. Drop Mixing in a Microchannel for Lab-on-a-Chip Platforms. *Langmuir* **2008**, *24*, 590–601.

(22) Pirbodaghi, T.; Vigolo, D.; Akbari, S.; deMello, A. Investigating the fluid dynamics of rapid processes within microfluidic devices using bright-field microscopy. *Lab Chip* **2015**, *15*, 2140–2144.

(23) Handique, K.; Burns, M. A. Mathematical modeling of drop mixing in a slit-type microchannel. *J. Micromech. Microeng.* **2001**, *11*, 548–554.

(24) Song, H.; Tice, J. D.; Ismagilov, R. F. A Microfluidic System for Controlling Reaction Networks in Time. *Angew. Chem., Int. Ed. Engl.* **2003**, *42*, 768–772.

(25) Blanchette, F.; Messio, L.; Bush, J. W. M. The influence of surface tension gradients on drop coalescence. *Phys. Fluids* **2009**, *21*, 072107.

(26) Karpitschka, S.; Riegler, H. Quantitative experimental study on the transition between fast and delayed coalescence of sessile droplets with different but completely miscible liquids. *Langmuir* **2010**, *26*, 11823–11829.

(27) Jehannin, M.; Charton, S.; Karpitschka, S.; Zemb, T.; Möhwald, H.; Riegler, H. Periodic Precipitation Patterns during Coalescence of Reacting Sessile Droplets. *Langmuir* **2015**, *31*, 11484–11490.

(28) Thoroddsen, S. T.; Qian, B.; Etoh, T. G.; Takehara, K. The initial coalescence of miscible drops. *Phys. Fluids* **2007**, *19*, 072110.

(29) Nowak, E.; Kovalchuk, N. M.; Che, Z.; Simmons, M. J. H. Effect of surfactant concentration and viscosity of outer phase during

DOI: 10.1021/acs.langmuir.9b00843
Langmuir 2019, 35, 9184–9193

the coalescence of a surfactant-laden drop with a surfactant-free drop. *Colloids Surf., A* **2016**, *505*, 124−131.
(30) Nowak, E.; Xie, Z.; Kovalchuk, N. M.; Matar, O. K.; Simmons, M. J. H. Bulk advection and interfacial flows in the binary coalescence of surfactant-laden and surfactant-free drops. *Soft Matter* **2017**, *13*, 4616−4628.
(31) Nash, J. J.; Spicer, P. T.; Erk, K. A. Controllable internal mixing in coalescing droplets induced by the solutal Marangoni convection of surfactants with distinct headgroup architectures. *J. Colloid Interface Sci.* **2018**, *529*, 224−233.
(32) Luo, X.; Yin, H.; Yan, H.; Huang, X.; Yang, D.; He, L. Electrocoalescence of Two Drops with Different Surfactant Concentrations Suspended in Oil. *J. Phys. Chem. C* **2018**, *122*, 22615−22621.
(33) Blanchette, F. Simulation of mixing within drops due to surface tension variations. *Phys. Rev. Lett.* **2010**, *105*, 074501.
(34) Kim, P.; Kwon, K. W.; Park, M. C.; Lee, S. H.; Kim, S. M.; Suh, K. Y. Soft lithography for microfluidics: a review. *BioChip J.* **2008**, *2*, 1−11.
(35) Schneider, C. A.; Rasband, W. S.; Eliceiri, K. W. NIH Image to ImageJ: 25 years of image analysis. *Nat. Methods* **2012**, *9*, 671−675.
(36) Buzzaccaro, S.; Secchi, E.; Piazza, R. Ghost particle velocimetry: accurate 3D flow visualization using standard lab equipment. *Phys. Rev. Lett.* **2013**, *111*, 048101.
(37) Riccomi, M.; Alberini, F.; Brunazzi, E.; Vigolo, D. Ghost Particle Velocimetry as an alternative to μPIV for micro/milli-fluidic devices. *Chem. Eng. Res. Des.* **2018**, *133*, 183−194.
(38) Kovalchuk, N. M.; Chowdhury, J.; Schofield, Z.; Vigolo, D.; Simmons, M. J. H. Study of drop coalescence and mixing in microchannel using Ghost Particle Velocimetry. *Chem. Eng. Res. Des.* **2018**, *132*, 881−889.
(39) Thielicke, W.; Stamhuis, E. J. PIVlab−Towards User-friendly, Affordable and Accurate Digital Particle Image Velocimetry in MATLAB. *J. Open Res. Softw.* **2014**, *2*, No. e30.
(40) Aksenenko, E. V. Software tools to interpret the thermodynamics and kinetics of surfactant adsorption. In *Surfactants—Chemistry, Interfacial Properties and Application. Studies in Interface Science*; Fainerman, V. B., Moebius, D., Miller, R., Eds.; Elsevier, 2001.
(41) Aksenenko, E. V. website http://www.thomascat.info/scientific/adso/adso.htm.
(42) Paulsen, J. D.; Carmigniani, R.; Kannan, A.; Burton, J. C.; Nagel, S. R. Coalescence of bubbles and drops in an outer fluid. *Nat. Commun.* **2014**, *5*, 3182.
(43) Lucassen, J.; van den Tempel, M. Dynamic measurements of dilational properties of a liquid interface. *Chem. Eng. Sci.* **1972**, *27*, 1283−1291.
(44) Mucic, N.; Javadi, A.; Kovalchuk, N. M.; Aksenenko, E. V.; Miller, R. Dynamics of interfacial layers-experimental feasibilities of adsorption kinetics and dilational rheology. *Adv. Colloid Interface Sci.* **2011**, *168*, 167−178.
(45) Yoshida, N.; Matsuoka, K.; Moroi, Y. Micelle Formation ofn-Decyltrimethylammonium Perfluorocarboxylates. *J. Colloid Interface Sci.* **1997**, *187*, 388−395.
(46) Villetti, M. A.; Borsali, R.; Crespo, J. S.; Soldi, V.; Fukada, K. Static and Dynamic Light Scattering of Polyelectrolyte/Surfactant Solutions: the Na-Hyaluronate/(C10TAB) System. *Macromol. Chem. Phys.* **2004**, *205*, 907−917.
(47) Rodríguez, J. L.; Sierra, M. B.; Messina, P. V.; Morini, M. A.; Schulz, P. C.; del Burgo, P.; et al. Surface and bulk properties of aqueous decyltrimethylammonium bromide-hexadecyltrimethylammonium bromide mixed system. *J. Colloid Interface Sci.* **2007**, *314*, 699−706.
(48) Kovalchuk, N. M.; Vollhardt, D. Theoretical description of repeated surface-tension auto-oscillations. *Phys. Rev. E: Stat., Nonlinear, Soft Matter Phys.* **2002**, *66*, 026302.
(49) Eggers, J.; Lister, J. R.; Stone, H. A. Coalescence of liquid drops. *J. Fluid Mech.* **1999**, *401*, 293−310.
(50) Mao, X.; Juluri, B. K.; Lapsley, M. I.; Stratton, Z. S.; Huang, T. J. Milliseconds microfluidic chaotic bubble mixer. *Microfluid. Nanofluid.* **2010**, *8*, 139−144.

DOI: 10.1021/acs.langmuir.9b00843
Langmuir 2019, 35, 9184−9193